Eur. Phys. J. B (2014) 87: 31
DOI: 10.1140/epjb/e2014-41064-y

THE EUROPEAN PHYSICAL JOURNAL B

Regular Article

Spectra of delay-coupled heterogeneous noisy nonlinear oscillators

Andrea Vüllings[1,a], Eckehard Schöll[1], and Benjamin Lindner[2,3]

[1] Institut für Theoretische Physik, TU Berlin, Hardenbergstraße 36, 10623 Berlin, Germany
[2] Physics Department, Humboldt University Berlin, Newtonstr. 15, 12489 Berlin, Germany
[3] Bernstein Center for Computational Neuroscience Berlin, HU Berlin, Philippstraße 13, 10115 Berlin, Germany

Received 30 November 2013 / Received in final form 21 December 2013
Published online 3 February 2014 –

Abstract. Nonlinear oscillators that are subject to noise and delayed interaction have been used to describe a number of dynamical phenomena in Physics and beyond. Here we study the spectral statistics (power and cross-spectral densities) of a small number of noisy nonlinear oscillators and derive analytical approximations for these spectra. In our paper, individual oscillators are described by the normal form of a supercritical or subcritical Hopf bifurcation supplemented by Gaussian white noise. Oscillators can be distinguished from each other by their frequency, bifurcation parameter, and noise intensity. Extending previous results from the literature, we first calculate in linear response theory the power spectral density and response function of the single oscillator in both super- and subcritical parameter regime and test them against numerical simulations. For small heterogeneous groups of oscillators ($N = 2$ or 3), which are coupled by a delayed linear term, we use a linear response ansatz to derive approximations for the power and cross-spectral densities of the oscillators within this small network. These approximations are confirmed by comparison with extensive numerical simulations. Using the theory we relate the peaks in the spectra of the homogeneous system (identical oscillators) to periodic solutions of the deterministic (noiseless) system. For two delay-coupled subcritical Hopf oscillators, we show that the coupling can enhance the coherence resonance effect, which is known to occur for the single subcritical oscillator. In the case of heterogeneous oscillators, we find that the delay-induced characteristic profile of the spectra is conserved for moderate frequency detuning.

1 Introduction

Nonlinear oscillators, which are coupled with a temporal delay occur in various scientific fields, such as laser physics [1], neuroscience [2] and developmental biology [3]. Systems with time delay generally possess stable and unstable periodic solutions, which can coexist in phase space [4]. This feature of time delay yields different in-phase and out-of phase periodic solutions, e.g., for delay-coupled Kuramoto oscillators [5], Stuart-Landau oscillators [6], semiconductor lasers [1] or neurons [7].

In many of the above systems, fluctuations influence the dynamics strongly and have to be taken into account. In a stochastic setting, oscillations of a finite coherence are characterized by peaks in the power spectral density, correlations between oscillators may also become apparent in cross-spectral peaks.

Remarkably, intrinsic or external fluctuations can induce oscillations in systems that are close to a bifurcation (but deterministically in a stable steady state). Oscillations are most pronounced at a finite noise intensity, an effect known as coherence resonance [8–14]. The control of noise-induced oscillations and coherence resonance, by using a delayed feedback loop in single (e.g. [15,16]) or coupled systems (e.g. [17,18]), has been investigated in various models.

Unfortunately, no standard technique exists to calculate or at least approximate spectral measures of coupled nonlinear oscillators if both noise and delay are involved. The aim of the current study is to put forward such an approximation scheme by combining recent analytical results on a generic oscillator model [19] with a simple network theory that has been successfully used in computational neuroscience [20–23]. The latter approximation procedure for power and cross-spectral densities can be applied to networks with and without time delay and to single systems with delayed self-feedback loop. It does not require a diagonalizable coupling matrix and can be used for heterogeneous networks with arbitrary local dynamics. The theory relies on the knowledge of quantities of the isolated (uncoupled) individual network elements (power spectrum and susceptibility with respect to periodic stimuli), which in general can be determined analytically, numerically, or experimentally, depending on the system under study.

Here we will consider small numbers of generic nonlinear oscillators (Hopf normal forms) which are subject to uncorrelated noise and are coupled by delay terms. We derive analytical approximations for power and

[a] e-mail: andreav@itp.tu-berlin.de

cross-spectral densities that are based on the spectral properties of the uncoupled system and the Fourier transform of the coupling term. For the single oscillator we will not only use the expressions for the supercritical normal form as given in reference [19] but also derive and use approximations for the subcritical normal form.

When interpreting our results for the spectral measures, we also compare them to oscillation patterns observed in the deterministic case. As mentioned above, the time delay induces certain deterministic periodic solutions or oscillation patterns, which can coexist in phase space. With noise, and depending on the noise intensity, a system can jump between such deterministic solutions and, thus, the power spectrum exhibits resonance peaks at different frequencies (see for example [15,17,24]). Within a time series, one can observe noise-induced transitions between these delay-induced periodic solutions. We relate the characteristic peaks of the power spectral density and cross-spectral densities to temporary oscillation patterns in the case of identical Hopf oscillators, and find that, in the case of heterogeneous oscillators, the characteristic profile of the spectra survives if the frequency detuning between the oscillators does not become too large. Moreover, the regularity of the temporary noisy oscillation patterns can be increased, for a non-zero amount of noise, for subcritical Hopf normal forms, which constitutes a manifestation of coherence resonance.

2 Model

We consider a network of systems, which are coupled by a delay term and subjected to independent Gaussian white noise. A single node of the network is described by a generic noisy oscillator, the normal form of a system close to a Hopf bifurcation and driven by white Gaussian noise. The corresponding stochastic differential equation for the kth node ($k = 1, 2, \ldots, N$) reads

$$\dot{z}_k(t) = \left[\lambda_k - i\omega_{0,k} + a|z_k(t)|^2 + b|z_k(t)|^4\right] z_k(t) + \sqrt{2D_k}\,\xi_k(t) + \sigma e^{i\beta} \sum_{j=1}^{N} G_{kj} z_j(t-\tau). \quad (1)$$

The dynamics of the complex-valued state variable $z_k \in \mathbb{C}$ is characterized by the bifurcation parameter λ_k and the intrinsic frequency $\omega_{0,k}$. In the absence of noise ($D_k = 0$) and coupling ($\sigma = 0$), the remaining deterministic part represents the normal form of a supercritical Hopf bifurcation if $a = -1$ and $b = 0$ (Fig. 1a) or that of a subcritical Hopf bifurcation if $a = 1$ and $b = -1$ (Fig. 1b). Such bifurcations can occur in various systems, e.g., in lasers [12,25], chemical reaction systems [26,27], neurons [28–30] and mechanosensory hair cells of the inner ear [31,32].

In order to model a noisy environment or internal stochastic processes, each oscillator is influenced by independent Gaussian white noise $\xi_k(t) = \xi_{k,1}(t) + i\,\xi_{k,2}(t)$ with noise intensity D_k, zero mean $\langle \xi_{k,l}(t) \rangle = 0$, for all k and $l = 1, 2$, and no correlation between the noise of different nodes and the real and imaginary part of $\xi_k(t)$, i.e., $\langle \xi_{k,l}(t)\, \xi_{j,m}(t') \rangle = \delta_{kj}\delta_{lm}\delta(t-t')$. Note that in general oscillators possess different parameters λ_k, $\omega_{0,k}$ and D_k, i.e., we deal with a heterogeneous network.

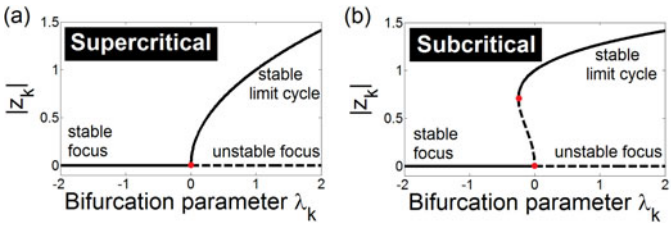

Fig. 1. Bifurcation diagram: (a) supercritical Hopf normal form (Eq. (1), where $a = -1$, $b = \sigma = D_k = 0$). (b) Subcritical Hopf normal form with an additional quintic term (Eq. (1), where $a = 1$, $b = -1$, $\sigma = D_k = 0$).

The oscillators are coupled via the coupling matrix (G_{kj}); $\sigma e^{i\beta}$ is a complex coupling coefficient with amplitude σ and phase β, and $\tau > 0$ denotes the time delay. Such a coupling scheme is adequate, for example, if lasers are coupled through optical fibers or mirrors [1,33]. By setting $\beta = 0$ and adding a term $-\sigma \sum_{j=1}^{N} G_{kj} z_k(t)$ in equation (1), the resulting network can be used, for instance, to model the connection between neurons with electrical synapses (gap junctions) [34].

In the next section, we discuss a procedure of how one can derive analytical approximations of the spectral properties of the system equation (1), namely the power spectral density $S_{kk}(\omega)$ of network node z_k and the cross-spectral densities $S_{kj}(\omega)$ ($k \neq j$) between different nodes of the network, by only using properties of the uncoupled system.

3 Theory

The power spectrum, or more precisely power spectral density (PSD), $S_{kk}(\omega)$ of the kth network node is defined as:

$$S_{kk}(\omega) = \lim_{T\to\infty} \frac{\langle \hat{z}_k(\omega)\hat{z}_k^*(\omega)\rangle}{T}, \quad (2)$$

where $\hat{z}_k(\omega) = \int_0^T e^{i\omega t} z_k(t)\, dt$ is the Fourier transform of the state $z_k(t)$, the symbol $*$ denotes complex conjugation, and the bracket $\langle\cdot\rangle$ denotes the average over the noise ensemble. The PSD contains information about the frequency content of $z_k(t)$ and is, thus, particularly suitable for indicating periodicity.

In contrast to the PSD, the cross-spectral densities (CS) $S_{kj}(\omega)$ comprise information about the degree of phase correlation between different nodes. The CS is analogously defined by

$$S_{kj}(\omega) = \lim_{T\to\infty} \frac{\left\langle \hat{z}_k(\omega)\hat{z}_j^*(\omega)\right\rangle}{T}, \quad k \neq j. \quad (3)$$

Both quantities can help us to detect, for example, a (temporary) stochastic phase-locked or in-phase state of the network, where all nodes exhibit noisy oscillations with zero mean-phase difference among each other (Fig. 2).

$$\Lambda_k = -\frac{2}{\langle\rho^2\rangle^2}\frac{a\left(\langle\rho\rangle\langle\rho^5\rangle\langle\rho^2\rangle - \langle\rho\rangle\langle\rho^4\rangle\langle\rho^3\rangle\right) + b\left(\langle\rho\rangle\langle\rho^7\rangle\langle\rho^2\rangle - \langle\rho\rangle\langle\rho^6\rangle\langle\rho^3\rangle\right) - D_k\left(\langle\rho^{-1}\rangle\langle\rho^2\rangle\langle\rho^3\rangle - \langle\rho^2\rangle^2\right)}{\lambda_k\left(\langle\rho^2\rangle - \langle\rho^{-1}\rangle\langle\rho^3\rangle\right) + a\left(\langle\rho^4\rangle - \langle\rho^{-1}\rangle\langle\rho^5\rangle\right) + b\left(\langle\rho^6\rangle - \langle\rho^{-1}\rangle\langle\rho^7\rangle\right)} \tag{10}$$

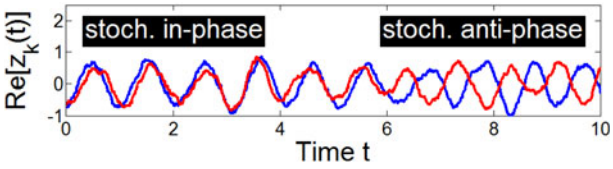

Fig. 2. Exemplary time series of two delay-coupled noisy supercritical Hopf normal forms: $\mathrm{Re}[z_1(t)]$ (red) and $\mathrm{Re}[z_2(t)]$ (blue). Switch from a stochastic in-phase state to a stochastic anti-phase state. Parameters: $\lambda_1 = \lambda_2 = -0.4$, $\omega_{0,1} = \omega_{0,2} = 2\pi$, $a = -1$, $b = 0$, $\sigma = 1$, $\beta = 0$, $\tau = 20T_0$, where $T_{0,k} = 2\pi/\omega_{0,k}$ is the intrinsic period.

Another example of an oscillation pattern of the network nodes is a (temporary) stochastic splay state, which is characterized by a fixed mean-phase difference between the oscillators. For instance, a stochastic anti-phase state is a splay state with mean-phase difference π between two oscillators. Figure 2 shows a transition between these two states of stochastic synchronization and anti-synchronization.

As in [21], we make the linear-response ansatz

$$\hat{z}_k(\omega) = \hat{z}_{k,0}(\omega) + \chi_{k,0}(\omega)\sum_{j=1}^{N}\sigma e^{i(\beta+\omega\tau)}G_{kj}\hat{z}_j(\omega), \tag{4}$$

where $\hat{z}_{k,0}(\omega)$ is the Fourier transform of the state $z_{k,0}(t)$ and $\chi_{k,0}(\omega)$ is the susceptibility of the kth uncoupled node (the index 0 indicates no coupling, i.e., $\sigma = 0$ in Eq. (1)). Conveniently, in the frequency domain, the delay in the coupling is simplified to a prefactor $e^{i\omega\tau}$. In equation (4) the interaction with the other oscillators is treated as a perturbation that can be captured at the level of the stochastic realization by the linear response function (or, equivalently, by the susceptibility) of the time-dependent mean value of the single oscillator. The ansatz equation (4) is suitable for networks with linear coupling function in the limit of weak coupling and was already successfully used for noisy leaky integrate-and-fire (LIF) neurons with global delayed feedback [21] and for arbitrary networks of LIF neurons [22].

The ansatz equation (4) constitutes a linear system of equations, for which the matrix of power and cross-spectral densities is obtained as [22]

$$\bar{S} = (\mathbb{1} - \bar{F})^{-1}\bar{S}^0[(\mathbb{1} - \bar{F}^*)^{-1}]^T, \tag{5}$$

in terms of a matrix $\bar{F}$, the elements of which are given by

$$\bar{F}_{kj}(\omega) = \chi_{k,0}\sigma e^{i(\beta+\omega\tau)}G_{kj}. \tag{6}$$

In equation (5) the superscript T denotes the transposed matrix, $\bar{S}_{kl} = S_{kl}(\omega)$ (power spectral density for $k = l$), and $\bar{S}^0_{kl} = \delta_{kl}S^0_{kk}$ is the matrix that has the spectra of the isolated oscillators on its diagonal and is otherwise zero. Below we will evaluate the general solution in two specific situations, yielding explicit expressions for the power and cross-spectral densities in the system.

The susceptibility $\chi_{k,0}(\omega)$ of the single oscillator can be computed from the linear response to a weak periodic or broadband stimulus $s(t)$. In the latter case, the susceptibility is given as the ratio of the input-output cross-spectrum and power spectrum of the input signal

$$\chi_{k,0}(\omega) = \lim_{\langle s^2\rangle\to 0}\lim_{T\to\infty}\frac{\langle\hat{x}_k\hat{s}^*\rangle}{\langle\hat{s}\hat{s}^*\rangle} \tag{7}$$

and the second limit indicates that we should compute the spectra in the limit of weak stimulation.

Based on the procedure proposed in [19], one can approximate the susceptibility $\chi_{k,0}(\omega)$ and power spectrum S^0_{kk} of the isolated Hopf oscillator as follows:

$$\chi_{k,0}(\omega) = \frac{1}{i\Lambda_k(\omega_{0,k} - \omega) + K_k}, \tag{8}$$

$$S^0_{kk} = \frac{4D_k\Lambda_k}{K_k^2 + \Lambda_k^2(\omega_{0,k} - \omega)^2}, \tag{9}$$

see equation (10) *above*,

$$K_k = \frac{2D_k}{\langle\rho^2\rangle}, \tag{11}$$

$$\langle\rho^n\rangle = \frac{\int_0^\infty d\rho\ \rho^{n+1}e^{-W_k/D_k}}{\int_0^\infty d\rho\ \rho e^{-W_k/D_k}}, \tag{12}$$

$$W_k = -\left(\frac{\lambda_k}{2}\rho^2 + \frac{a}{4}\rho^4 + \frac{b}{6}\rho^6\right). \tag{13}$$

The above equations were already derived in reference [19] for the case $b = 0$ (supercritical case). In the low noise limit ($D \to 0$), the moments in Λ_k and K_k can be simplified by means of a saddle-point approximation (for details we refer the interested reader to [19,35]). We will, however, use the full expressions and calculate the integrals numerically. For analytical results on the nonlinear response of the stochastic Hopf oscillator in the case of strong periodic stimulation, see [36].

Before discussing some results for specific network motifs, we will compare the theoretical results for S^0_{kk} and $\chi_{k,0}$ with numerical simulations on the one hand, and, on the other hand, with an alternative approximation of S^0_{jj} [12].

4 Testing the theory with numerical simulation

4.1 One isolated oscillator

In order to approximate the spectral properties of a coupled system, we need a good approximation of the PSD

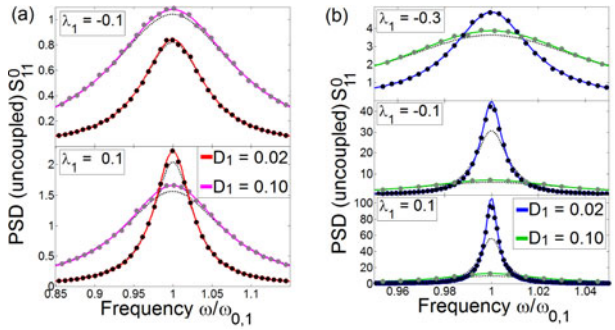

Fig. 3. Power spectral density (PSD) of (a) a supercritical and (b) subcritical Hopf normal form for different bifurcation parameters λ_1 and noise intensities D_1. The symbols correspond to numerical simulations, the solid lines display the analytical results (Eq. (9)), and the black dotted lines represent the analytical result from reference [12]. Parameters: $\omega_{0,1} = 2\pi$, $\sigma = 0$, in (a) $a = -1$, $b = 0$ and in (b) $a = 1$, $b = -1$.

$S^0_{11}(\omega)$ and susceptibility $\chi_{1,0}(\omega)$ of the uncoupled system ($\sigma = 0$ and $N = 1$ in Eq. (1)).

Starting with the power spectrum, Figure 3 shows the numerical results (symbols) and the approximation (solid line) of $S^0_{11}(\omega)$ equation (9) for different bifurcation parameters λ_1 and noise intensities D_1. Figure 3a corresponds to the supercritical and Figure 3b to the subcritical Hopf normal form. In all cases, the theoretical results agree with the results of numerical simulations. The black dotted lines correspond to an approximation of reference [12], which becomes equivalent to ours if $\Lambda_1 \equiv 1$. The authors of [12] derived their approximation for small noise intensity and closely below the first deterministic bifurcation point λ_c ($\lambda_c = 0$ and $\lambda_c = 0.25$ in the supercritical or subcritical case, respectively, see also Fig. 1). For such a choice of parameters, the numerical results (symbols) are in good agreement with their approximation (black dotted lines). However, for larger noise intensities and above λ_c, the numerical results emphasize that Λ_1, which contains higher-order moments, becomes important for the stochastic dynamics of the uncoupled system. In this case, our approximation provides a more appropriate estimate. For $\lambda > \lambda_c$, in the deterministic regime of a stable limit cycle, the resonance peaks of both oscillator types correspond to noisy self-sustained oscillations. The higher the noise intensity, the broader the resonance peaks become. In this regime, noise diminishes the coherence of the oscillations.

For $\lambda < \lambda_c$, in the regime of noise-induced oscillations, the dependence of the peak height and peak width of the PSD on noise differs qualitatively for the two types of bifurcations (see Fig. 4). While in the supercritical case the height and width of the PSD is a monotonic function of the noise intensity, the PSD of the subcritical case behaves non-monotonically [12]. In the latter case, if the peak height is maximal and the peak width is minimal for a certain optimal amount of noise, the noise-induced oscillation achieves the highest degree of regularity. This interplay between noise and nonlinearity is called coherence resonance (see, e.g., [8,10,12,14] for a more detailed discussion).

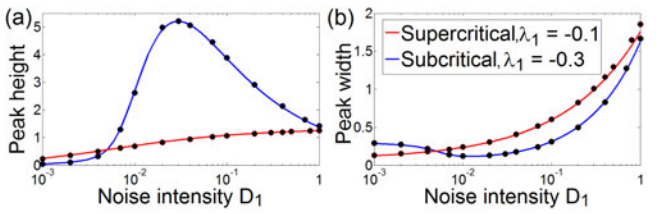

Fig. 4. Theoretical (solid lines) and numerical results (symbols) of (a) the peak height and (b) the peak width of S^0_{11} (Eq. (9)). Parameters: $\omega_{0,1} = 2\pi$, $\sigma = 0$, for the supercritical case (red) $a = -1$, $b = 0$ and subcritical case (blue) $a = 1$, $b = -1$.

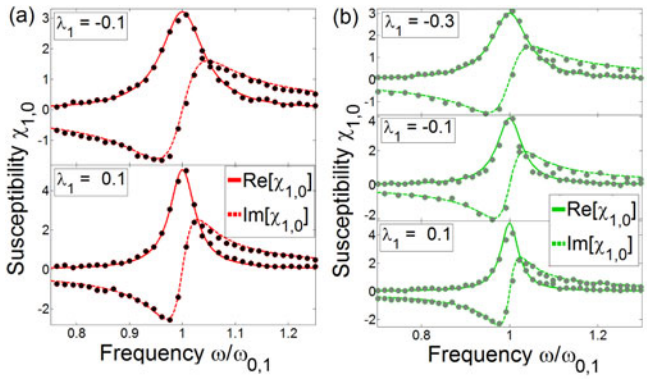

Fig. 5. Susceptibility $\chi_{1,0}(\omega)$ of (a) a supercritical (red), where $D_1 = 0.01$, and (b) subcritical (green) Hopf normal form, where $D_1 = 0.1$. The symbols correspond to numerical simulations, the solid lines display the analytical results (Eq. (8)) of the real part and the dashed lines of the imaginary part of $\chi_{1,0}(\omega)$. Parameters: $\omega_{0,1} = 2\pi$, $\sigma = 0$, in (a) $a = -1$, $b = 0$ and in (b) $a = 1$, $b = -1$.

Finally, Figure 5 shows that the simulations (symbols) and the analytical estimates (solid and dashed lines) of the real and imaginary part of the susceptibility $\chi_{1,0}(\omega)$ (Eq. (8)) are in good agreement. We have tested the validity of our approximations for a range of noise intensities and found deviations from the simulations if the noise intensity D_1 becomes too large (i.e., if $D_1 = \mathcal{O}(1)$).

Now that we have seen how reliable the approximations are, and how the local spectral properties of a single node are influenced by noise, we consider small network motifs of coupled oscillators.

4.2 Two symmetrically coupled oscillators

From the general result equation (5) stated above, we can obtain explicit results by choosing a specific topology. For the example of a symmetric (2×2)-coupling matrix

$$(G_{kj}) = \begin{pmatrix} 0 & 1 \\ 1 & 0 \end{pmatrix}, \tag{14}$$

the analytical results for power and cross-spectral densities are given in Appendix A.

For identical oscillators, it holds that $\chi_{1,0} = \chi_{2,0} \equiv \chi_0(\omega)$ (Eq. (8)) and $S^0_{11} = S^0_{22} \equiv S_0(\omega)$ (Eq. (9)).

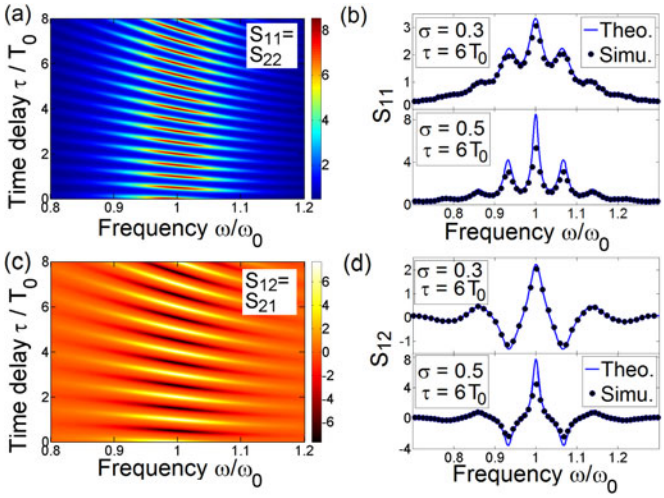

Fig. 6. Two delay-coupled identical subcritical Hopf normal forms in the regime of noise-induced oscillations: theoretical result (Eq. (15)) of (a) the power spectral density (PSD) and (c) the cross-spectrum (CS) in the (ω, τ)-plane. Panel (b) shows the theoretical and numerical result of the PSD and (d) of the CS for a fixed time delay τ and for two different coupling strengths σ. Parameters: $\lambda_1 = \lambda_2 = -0.4$, $\omega_{0,1} = \omega_{0,2} \equiv \omega_0 = 2\pi$, $a = 1$, $b = -1$, $\sigma = 0.5$, $\beta = 0$, $D_1 = D_2 \equiv D = 0.3$ and $T_0 = 2\pi/\omega_0$.

Then, the PSD and CS in Appendix A simplify significantly and are given by

$$S_{kk}(\omega) = g(\omega)S_0(\omega), \quad S_{kj}(\omega) = h(\omega)S_0(\omega), \tag{15}$$

where

$$g(\omega) = \frac{1 + |\chi_0|^2\sigma^2}{1 + |\chi_0|^4\sigma^4 - 2|\chi_0|^2\sigma^2\cos[2\alpha]},$$
$$h(\omega) = \frac{2|\chi_0|\sigma\cos[\alpha]}{1 + |\chi_0|^4\sigma^4 - 2|\chi_0|^2\sigma^2\cos[2\alpha]}$$

and $\alpha = \omega\tau + \beta + \arg(\chi_0)$. The PSD S_{kk} and CS S_{kj} of the coupled system depend on the PSD S_0 of the uncoupled system and are scaled by the functions g and h, which contain the susceptibility χ_0 and the coupling parameters σ, β and τ. The cosine function in g and h implies that the coupling induces periodicity.

For identical subcritical oscillators in the regime of noise-induced oscillations, Figure 6 shows theoretical and numerical results for S_{kk} and S_{kj}, where $k, j = 1, 2$ and $k \neq j$. As expected, the spectra exhibit repetitive maxima and minima. Similar spectra have been observed theoretically in single and coupled systems, which operate in the regime of noise-induced oscillations [15–17,24,37,38] and experimentally in coupled lasers [1,39,40]. In our model, the characteristic profile of the spectra does not change qualitatively if we replace the subcritical oscillators by supercritical ones, or if we poise the bifurcation parameters λ in the regime of self-sustained oscillations. For moderate coupling strengths, i.e., if $0 > \sigma > 0.5$, our approximation of the spectra is in good agreement with the numerical simulations (see for example Figs. 6b and 6d).

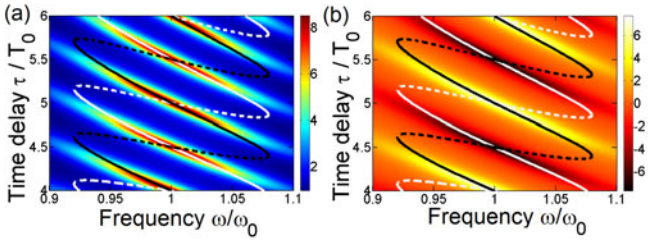

Fig. 7. For the same example given in Figure 6, (a) shows the PSD $S_{11} = S_{22}$ and (b) the CS $S_{12} = S_{21}$ together with the deterministic in-phase (black lines, Eq. (16)) and anti-phase solution (white lines, Eq. (17)) in the (ω, τ)-plane. The dashed lines indicate unstable solutions and the solid lines indicate stable solutions. Parameters: see Figure 6.

Generally, for two mutually delay-coupled Hopf normal forms without noise, multiple branches of in- and anti-phase periodic solutions appear [4,5]. In our case, the rotating wave ansatz (i) $z_1 = z_2 = re^{i\omega t}$ (in-phase solution) and (ii) $z_1 = -z_2 = re^{i\omega t}$ (anti-phase solution) satisfies equation (1), where $D_k = 0\ \forall k$, $N = 2$, $\lambda_1 = \lambda_2$, $\omega_{0,1} = \omega_{0,2} \equiv \omega_0$ if

$$\text{for (i):} \quad \omega = \omega_0 + \sigma\sin(\beta - \omega\tau), \tag{16}$$
$$\text{for (ii):} \quad \omega = \omega_0 - \sigma\sin(\beta - \omega\tau). \tag{17}$$

In Figure 7, the time delays τ and frequencies ω for possible oscillation patterns of the two deterministic oscillators are plotted on top of the PSD and CS. The black lines correspond to the deterministic in-phase solution and the white lines correspond to the deterministic anti-phase solution. The comparison shows that, if we add noise (a perturbation), not all deterministic solutions appear as resonance peaks in the spectra. The branches, which do not occur in the spectra, are apparently unstable and thus denoted by dashed lines in Figure 7. In addition, we also see peaks at frequencies that are not present in the deterministic case, namely, those at $\omega = 0.87$ and $\omega = 1.13$ in Figure 6b. These peaks can be understood as resulting from a noise-induced broadening of the spectral maxima in the (ω, τ)-plane, shown in Figure 7.

When we compare the deterministic solutions with the spectra, we can relate the resonance peaks in the spectra at a fixed time delay and frequency to a certain oscillation pattern, which the system shows for a limited time: for example, the primary resonance peak in the PSD (Fig. 7a) for $\omega = \omega_0$ and

$$\tau = nT_0, \tag{18}$$

where $n = 0, 1, 2, \ldots$ and $T_0 = 2\pi/\omega_0$ is the intrinsic oscillation frequency, corresponds to *(temporary) stochastic in-phase oscillations*. For the same parameters, the CS exhibits maximal correlation (Fig. 7b). In contrast to this, the CS exhibits strong anti-correlation and the PSD is maximal at $\omega = \omega_0$ and for

$$\tau = \left(\frac{1}{2} + n\right)T_0. \tag{19}$$

Here, the primary resonance peak corresponds to *(temporary) stochastic anti-phase oscillations*.

In the deterministic case, the time-delay induces in- and anti-phase solutions, which coexist for large delays (see Fig. 7). On the one hand, with noise, the system can jump between those oscillation patterns, which thus become visible as secondary peaks in the PSD and CS. On the other hand, the branches of in- and anti-phase solutions are smeared out due to the noise and thus appear as remaining peaks at the edge of the spectra (see Figs. 6b and 6d). This characteristic of the system is independent of the bifurcation parameter λ (compare also Eqs. (16) and (17) which is independent of λ) and can be observed in the regime of noise-induced oscillations, as well as in the regime of noisy self-sustained oscillations. For large delay, within a sufficiently long time series, one can observe jumps between the different noisy oscillation patterns (see for example Fig. 2).

In the uncoupled system, we already observed coherence resonance for the subcritical Hopf oscillator closely below the saddle-node bifurcation (see Fig. 3) in accordance with the results from [12]. This was indicated by a non-monotonic behavior of the height and width of the peak in the power spectrum for increasing noise intensity. Now, in the coupled system of two identical oscillators, one can observe the same phenomenon. Figures 8a, 8d and 8b, 8e show the height and width of the primary resonance peak of the power spectrum at $\omega = \omega_0$ as functions of the noise intensity for a fixed delay τ and different coupling strengths σ. Remarkably, for stronger coupling (larger σ), peak height and width show a more pronounced maximum and minimum, respectively. This can be interpreted as an enhancement of coherence resonance due to the delayed coupling. With increasing coupling strength the optimal noise at which maximal peak height is attained, shifts to smaller values. The coupling does not affect much the optimal noise intensity at which the peak width is minimized, although there is an overall reduction in peak width with increasing coupling strength σ. Also, with growing σ the deviation between our theoretical and numerical results increases, in particular, with respect to the peak height (theory is expected to work best for weak coupling). However, the theory still predicts the qualitative changes that occur in the spectral characteristics upon changing the coupling.

For $\sigma = 0.3$ the appearance of coherence resonance is illustrated by the trajectories at different noise values in Figures 8c and 8f. At intermediate noise intensity $D = 0.05$ the most regular oscillations in both coupled oscillators are observed. Note that we did not observe coherence resonance for the delay-coupled system in the case of supercritical Hopf oscillators, similar to what was found for the isolated oscillator.

The theory of the deterministic in- and anti-phase solutions (Eqs. (16) and (17)) predicts that, for coupling phase parameters $\beta \neq 0$, the branches experience a frequency shift. This prediction agrees with the analytical and numerical results of the spectra (see Fig. 9). For example, for $\tau = 4T_0$ and $\beta = 0, 2\pi$, the primary resonance peak at $\omega = \omega_0$ in Figures 9a and 9c corresponds to a temporary and noisy in-phase oscillation pattern, whereas for

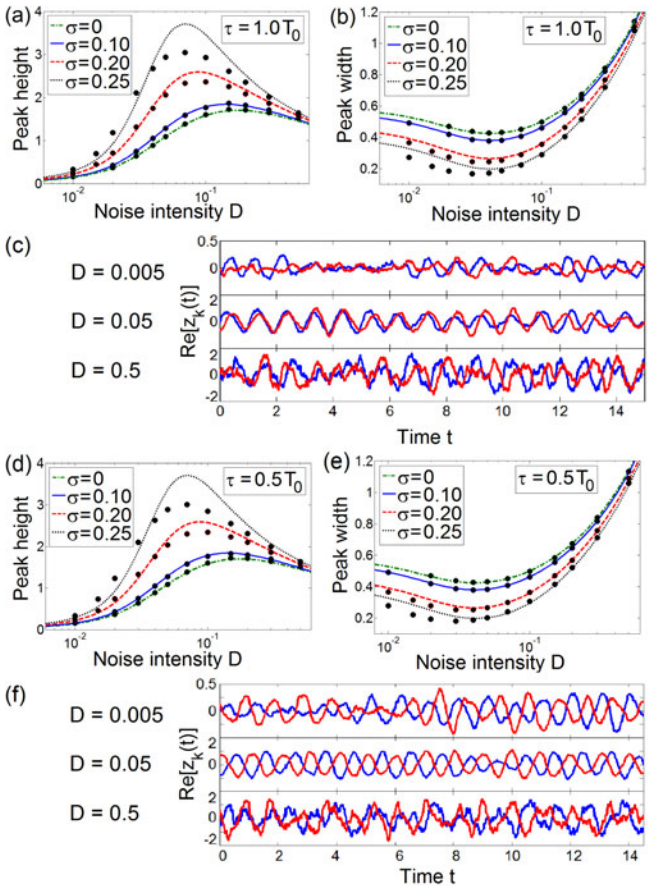

Fig. 8. Two delay-coupled identical subcritical Hopf oscillators in the regime of noise-induced oscillations: analytical (lines) and numerical results (symbols) of (a)+(d) the peak height and (b)+(e) the peak width of the primary resonance peak of the PSD $S_{11} = S_{22}$ at $\omega = \omega_0$ as a function of the noise intensity D for different coupling strengths σ. Here, the primary resonance peak for the metadata in (a) and (b) can be related to a stochastic in-phase oscillation pattern ($\tau = 1.0T_0$) and for the metadata in (d) and (e) the primary resonance peak belongs to a stochastic anti-phase oscillation pattern because $\tau = 0.5T_0$. (c)+(f) Time series of node 1 (red) and node 2 (blue) for different D and $\sigma = 0.3$, where the stochastic in-phase (and stochastic anti-phase) oscillation pattern exhibits its highest regularity (coherence resonance) for $D \neq 0$. Parameters: $\lambda_1 = \lambda_2 = -0.6$, $\omega_{0,1} = \omega_{0,2} \equiv \omega_0 = 2\pi$, $\beta = 0$, $a = 1$, $b = -1$, (c) $\tau = 1.0T_0$ and (f) $\tau = 0.5T_0$.

$\beta = \pi$ the primary resonance peak belongs to a temporary and noisy anti-phase oscillation.

In summary, many features of the spectra of noisy oscillators can be traced back to the delay-induced deterministic in- and anti-phase periodic solutions. We now turn to the case of heterogeneous oscillators and inspect how the spectral shapes discussed so far change.

Starting with randomly chosen parameters, Figures 10a and 10b show the power spectral density S_{11} of node 1 and S_{22} of node 2 in the ω-τ plane for two coupled non-identical Hopf normal forms. Figures 10c and 10d display the corresponding cross-spectra. Below each spectrum, one can see that our theoretical predictions (lines)

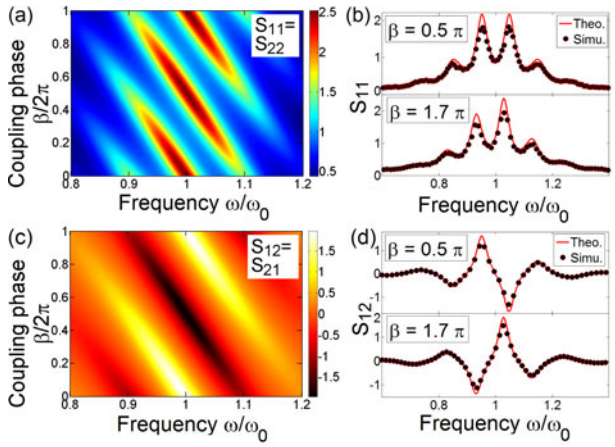

Fig. 9. Two delay-coupled identical supercritical Hopf normal forms: theoretical result (Eq. (15)) of (a) the PSD and (c) of the CS in the ω-β plane for $\tau = 4T_0$. (b) and (d) show the theoretical results (lines) and results of simulations (symbols) of the PSD and the CS for different coupling phases β. Parameters: $\lambda_1 = \lambda_2 = -0.1$, $\omega_{0,1} = \omega_{0,2} = 2\pi$, $a = -1$, $b = 0$, $\sigma = 0.5$, $\tau = 4T_0$ and $D_1 = D_2 = 0.3$.

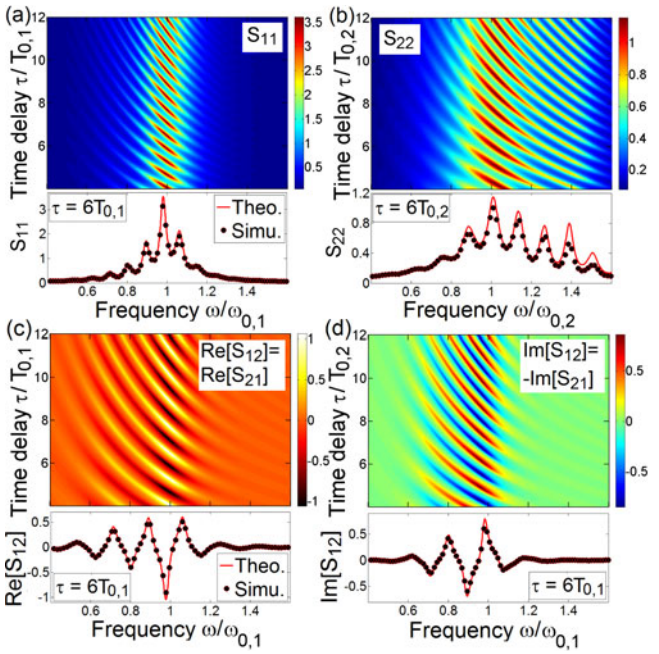

Fig. 10. Two delay-coupled non-identical supercritical Hopf normal forms: theoretical result (Appendix A) of (a) the PSD S_{11} and (b) S_{22}, (c) the real part of the CS $S_{12} = S_{21}$ and (d) the corresponding imaginary part of the CS in the (ω, τ)-plane. The theoretical results (lines) and results of simulations (symbols) of the spectra for a fixed time delay are shown below the corresponding spectra. Parameters: $\lambda_1 = -0.24$, $\lambda_2 = 0.47$, $\omega_{0,1} = 1.64\pi$, $\omega_{0,2} = 1.03\pi$, $D_1 = 0.351$, $D_2 = 0.253$, $\beta = 0.14\pi$, $\sigma = 0.6$, $a = -1$ and $b = 0$.

4.3 Three asymmetrically coupled oscillators

Next we use the general formula equation (5) to compute an approximation of the power spectral density (PSD) S_{kk} and the cross-spectrum (CS) S_{kj} of a directed ring network of three delay-coupled heterogeneous nonlinear oscillators whose coupling matrix,

$$(G_{ij}) = \begin{pmatrix} 0 & 1 & 0 \\ 0 & 0 & 1 \\ 1 & 0 & 0 \end{pmatrix}, \tag{20}$$

is asymmetric. The results for the PSD and CS are given in Appendix B.

For identical oscillators, it holds $\chi_{1,0} = \chi_{2,0} = \chi_{3,0} \equiv \chi_0(\omega)$ (Eq. (8)) and $S^0_{11} = S^0_{22} = S^0_{33} \equiv S_0(\omega)$ (Eq. (9)). Then, the PSD and CS in Appendix B simplify significantly and are given by

$$S_{kk}(\omega) = v(\omega) S_0(\omega), \quad S_{kj}(\omega) = w(\omega) S_0(\omega), \tag{21}$$

where

$$v(\omega) = \frac{1 + |\chi_0|^2\sigma^2 + |\chi_0|^4\sigma^4}{1 + |\chi_0|^6\sigma^6 - 2|\chi_0|^3\sigma^3\cos[3\alpha]},$$

$$w(\omega) = -\frac{e^{i\alpha}\sigma|\chi_0|\left(\sigma|\chi_0| + e^{3i\alpha}\left(1 + \sigma^2|\chi_0|^2\right)\right)}{\sigma^3|\chi_0|^3 + e^{6i\alpha}\sigma^3|\chi_0|^3 - e^{3i\alpha}\left(1 + \sigma^6|\chi_0|^6\right)}$$

and $\alpha = \omega\tau + \beta + \arg(\chi_0)$.

Figure 11 displays the theoretical and numerical results of the spectra for identical subcritical Hopf normal forms. As in the previous section, the resonance peaks can be related to deterministic delay-induced periodic solutions, which coexist in the phase space for larger τ. The rotating wave ansatz (i) $z_1 = z_2 = z_3 = re^{i\omega t}$ (in-phase solution); (ii) $z_1 = e^{-i2\pi/3}z_2 = e^{i2\pi/3}z_3 = re^{i\omega t}$ (splay state 1) and (iii) $z_1 = e^{i2\pi/3}z_2 = e^{-i2\pi/3}z_3 = re^{i\omega t}$ (splay state 2) satisfies equation (1), where $D_k = 0\ \forall k$, $N = 3$, $\lambda_1 = \lambda_2 = \lambda_3$, $\omega_{0,1} = \omega_{0,2} = \omega_{0,3} \equiv \omega_0$ if

$$\text{for (i):} \quad \omega = \omega_0 + \sigma\sin(\beta - \omega\tau), \tag{22}$$

$$\text{for (ii):} \quad \omega = \omega_0 + \sigma\sin(\beta + 2\pi/3 - \omega\tau), \tag{23}$$

$$\text{for (iii):} \quad \omega = \omega_0 + \sigma\sin(\beta - 2\pi/3 - \omega\tau). \tag{24}$$

The solutions of these equations are plotted, for $\tau \in [0, 2]$, in Figure 11c, which shows the real part of the CS in the (ω, τ)-plane. The CS exhibits the strongest correlation when the PSD (Fig. 11a) takes its maximum at $\omega = \omega_0$ (primary resonance peak) if

$$\tau = nT_0. \tag{25}$$

By comparing this with the deterministic solution (black line in Fig. 11c), we can relate these primary resonance peaks to *(temporary) stochastic in-phase oscillation*. The PSD is maximal at $\omega = \omega_0$ if

$$\tau = \left(\frac{1}{3} + n\right)T_0 \quad \text{or} \quad \tau = \left(\frac{2}{3} + n\right)T_0. \tag{26}$$

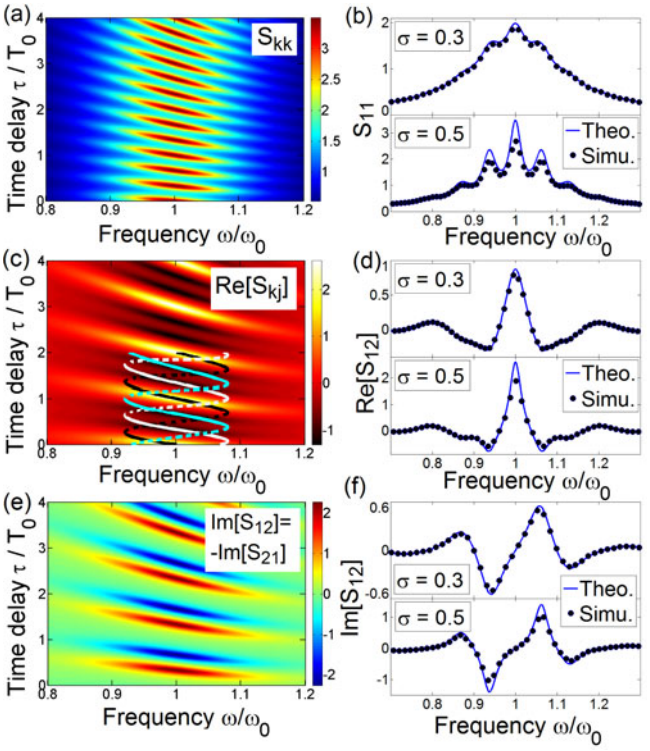

Fig. 11. Three delay-coupled identical subcritical Hopf normal forms: theoretical result (Appendix B) of (a) the PSD S_{kk}, (c) the real part of the CS S_{kj} together with the deterministic in-phase solution (black lines, Eq. (22)) and the two splay state solutions (white and blue lines, Eqs. (23) and (24)) in the (ω, τ)-plane. (e) Shows the theoretical result of the imaginary part of S_{12}. The theoretical results (solid lines) and results of simulations (symbols) of the spectra are shown in (b), (d) and (f) for $\tau = 4T_0$ and for two different coupling strengths σ. Parameters: $\lambda_1 = \lambda_2 = \lambda_3 = -0.6$, $\omega_{0,1} = \omega_{0,2} = \omega_{0,3} = 2\pi$, $a = 1$, $b = -1$, $\sigma = 0.5$, $\beta = 0$ and $D_1 = D_2 = D_3 = 0.3$.

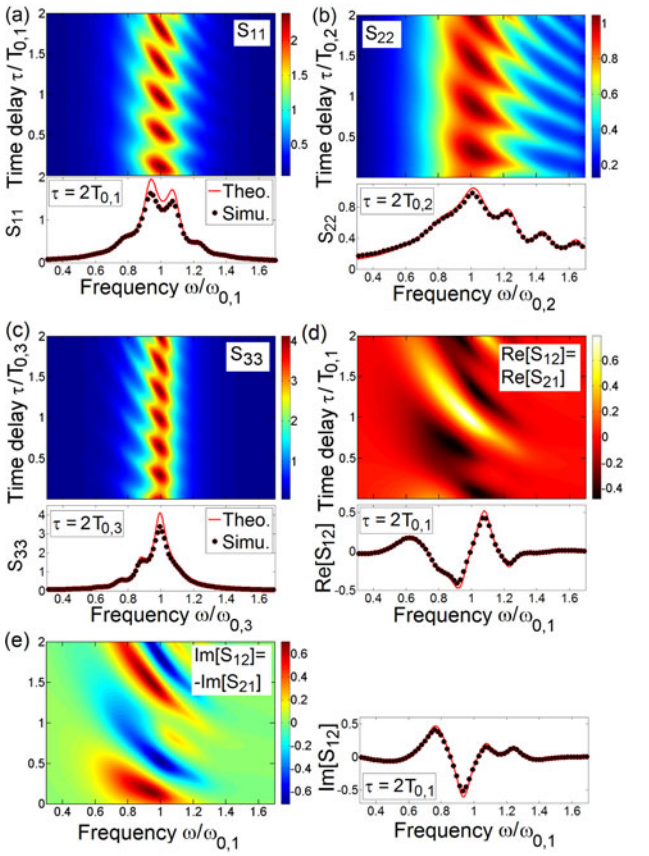

Fig. 12. Three delay-coupled non-identical supercritical Hopf normal forms: theoretical result (Appendix B) of (a) the PSD S_{11}, (b) S_{22}, (c) S_{33}, (d) the real part of the CS S_{12} and (e) the corresponding imaginary part of the CS in the (ω, τ)-plane. The theoretical results (lines) and results of simulations (symbols) of the spectra for a fixed time delay are shown below the corresponding and spectra. Parameters: $\lambda_1 = -0.24$, $\lambda_2 = 0.47$, $\lambda_3 = 0.56$, $\omega_{0,1} = 1.57\pi$, $\omega_{0,2} = 1.18\pi$, $\omega_{0,3} = 1.96\pi$, $D_1 = 0.174$, $D_2 = 0.260$, $D_3 = 0.247$, $\beta = 0.53\pi$, $\sigma = 0.6$, $a = -1$ and $b = 0$.

The comparison with the deterministic solutions (white and blue lines in Fig. 11c) shows that these primary resonance peaks correspond to *(temporary) stochastic splay states 1* and *2*.

For a network of heterogeneous supercritical Hopf oscillators, we compute the spectra shown in Figures 12a–12f and, as in the case of the two oscillators, despite the heterogeneities, the characteristic profile of the spectra is conserved and our approximation holds as long as the frequency detuning is moderate.

5 Conclusion

In this paper we have studied the spectral statistics of small network motifs of delay-coupled noisy nonlinear oscillators. In the first part of this work, following reference [19], we have derived approximations for the power spectral density and the susceptibility of a generic oscillator that are valid for weak noise and cover the cases in which the system is close to a supercritical or to a subcritical Hopf bifurcation. For the subcritical case, as a testbed for our theory, we have reproduced the phenomenon of coherence resonance (first discussed and analytically studied for this system in Ref. [12]), which is encountered for the system on the non-oscillating side of the bifurcation. We found that our theory also works well beyond the bifurcation as long as the noise intensity is not excessively large.

In the second part, an approximation of the power and cross-spectral densities for delay-coupled heterogeneous Hopf oscillators was derived and validated by numerical simulations of two or three oscillators. We have related the characteristic peaks of the spectra to delay-induced deterministic oscillation patterns, for example, to in- and anti-phase oscillations. The larger the time delay, the more peaks appear in the spectra. The heights and widths of resonance peaks can be non-monotonic functions of the noise intensity if we consider coupled subcritical Hopf oscillators implying coherence resonance. Here, for a non-zero optimal amount of noise, this specific noisy oscillation pattern can achieve highest coherence

$$
\begin{aligned}
S_{kk}(\omega) &= \frac{S^0_{kk} + S^0_{jj}\sigma^2|\chi_{k,0}|^2}{1+|\chi_{1,0}|^2|\chi_{2,0}|^2\sigma^4 - 2|\chi_{1,0}||\chi_{2,0}|\sigma^2\cos[2(\beta+\omega\tau)+\arg(\chi_{1,0})+\arg(\chi_{2,0})]},\\
\mathrm{Re}[S_{kj}](\omega) &= \frac{\sigma(|\chi_{k,0}|S^0_{jj}\cos[\beta+\omega\tau+\arg(\chi_{k,0})] + |\chi_{j,0}|S^0_{kk}\cos[\beta+\omega\tau+\arg(\chi_{j,0})])}{1+|\chi_{1,0}|^2|\chi_{2,0}|^2\sigma^4 - 2|\chi_{1,0}||\chi_{2,0}|\sigma^2\cos[2(\beta+\omega\tau)+\arg(\chi_{1,0})+\arg(\chi_{2,0})]},\\
\mathrm{Im}[S_{12}](\omega) = -\mathrm{Im}[S_{21}](\omega) &= \frac{\sigma(|\chi_{1,0}|S^0_{22}\sin[\beta+\omega\tau+\arg(\chi_{1,0})] - |\chi_{2,0}|S^0_{11}\sin[\beta+\omega\tau+\arg(\chi_{2,0})])}{1+|\chi_{1,0}|^2|\chi_{2,0}|^2\sigma^4 - 2|\chi_{1,0}||\chi_{2,0}|\sigma^2\cos[2(\beta+\omega\tau)+\arg(\chi_{1,0})+\arg(\chi_{2,0})]}
\end{aligned}
\tag{A.1}
$$

$$
\begin{aligned}
S_{11}(\omega) &= \frac{S^0_{11} + |\chi_{1,0}|^2\sigma^2(S^0_{22}+|\chi_{2,0}|^2S^0_{33}\sigma^2)}{1+|\chi_{1,0}|^2|\chi_{2,0}|^2|\chi_{3,0}|^2\sigma^6 - 2|\chi_{1,0}||\chi_{2,0}||\chi_{3,0}|\sigma^3\cos[3(\beta+\omega\tau)+\arg(\chi_{1,0})+\arg(\chi_{2,0})+\arg(\chi_{3,0})]},\\
S_{22}(\omega) &= \frac{S^0_{22} + |\chi_{2,0}|^2\sigma^2(S^0_{33}+|\chi_{3,0}|^2S^0_{11}\sigma^2)}{1+|\chi_{1,0}|^2|\chi_{2,0}|^2|\chi_{3,0}|^2\sigma^6 - 2|\chi_{1,0}||\chi_{2,0}||\chi_{3,0}|\sigma^3\cos[3(\beta+\omega\tau)+\arg(\chi_{1,0})+\arg(\chi_{2,0})+\arg(\chi_{3,0})]},\\
S_{33}(\omega) &= \frac{S^0_{33} + |\chi_{3,0}|^2\sigma^2(S^0_{11}+|\chi_{1,0}|^2S^0_{22}\sigma^2)}{1+|\chi_{1,0}|^2|\chi_{2,0}|^2|\chi_{3,0}|^2\sigma^6 - 2|\chi_{1,0}||\chi_{2,0}||\chi_{3,0}|\sigma^3\cos[3(\beta+\omega\tau)+\arg(\chi_{1,0})+\arg(\chi_{2,0})+\arg(\chi_{3,0})]},\\
\mathrm{Re}[S_{12}](\omega) &= \mathrm{Re}[S_{21}](\omega)\\
&= \frac{\sigma(|\chi_{1,0}|(S^0_{22}+|\chi_{2,0}|^2S^0_{33}\sigma^2)\cos[\beta+\omega\tau+\arg(\chi_{1,0})] + |\chi_{2,0}||\chi_{3,0}|S^0_{11}\sigma\cos[2(\beta+\omega\tau)+\arg(\chi_{2,0})+\arg(\chi_{3,0})])}{1+|\chi_{1,0}|^2|\chi_{2,0}|^2|\chi_{3,0}|^2\sigma^6 - 2|\chi_{1,0}||\chi_{2,0}||\chi_{3,0}|\sigma^3\cos[3(\beta+\omega\tau)+\arg(\chi_{1,0})+\arg(\chi_{2,0})+\arg(\chi_{3,0})]},\\
\mathrm{Im}[S_{12}](\omega) &= -\mathrm{Im}[S_{21}](\omega)\\
&= \frac{\sigma(|\chi_{1,0}|(S^0_{22}+|\chi_{2,0}|^2S^0_{33}\sigma^2)\sin[\beta+\omega\tau+\arg(\chi_{1,0})] - |\chi_{2,0}||\chi_{3,0}|S^0_{11}\sigma\sin[2(\beta+\omega\tau)+\arg(\chi_{2,0})+\arg(\chi_{3,0})])}{1+|\chi_{1,0}|^2|\chi_{2,0}|^2|\chi_{3,0}|^2\sigma^6 - 2|\chi_{1,0}||\chi_{2,0}||\chi_{3,0}|\sigma^3\cos[3(\beta+\omega\tau)+\arg(\chi_{1,0})+\arg(\chi_{2,0})+\arg(\chi_{3,0})]},\\
\mathrm{Re}[S_{23}](\omega) &= \mathrm{Re}[S_{32}](\omega)\\
&= \frac{\sigma(|\chi_{2,0}|(S^0_{33}+|\chi_{3,0}|^2S^0_{11}\sigma^2)\cos[\beta+\omega\tau+\arg(\chi_{2,0})] + |\chi_{1,0}||\chi_{3,0}|S^0_{22}\sigma\cos[2(\beta+\omega\tau)+\arg(\chi_{1,0})+\arg(\chi_{3,0})])}{1+|\chi_{1,0}|^2|\chi_{2,0}|^2|\chi_{3,0}|^2\sigma^6 - 2|\chi_{1,0}||\chi_{2,0}||\chi_{3,0}|\sigma^3\cos[3(\beta+\omega\tau)+\arg(\chi_{1,0})+\arg(\chi_{2,0})+\arg(\chi_{3,0})]},\\
\mathrm{Im}[S_{23}](\omega) &= -\mathrm{Im}[S_{32}](\omega)\\
&= \frac{\sigma(|\chi_{2,0}|(S^0_{33}+|\chi_{3,0}|^2S^0_{11}\sigma^2)\sin[\beta+\omega\tau+\arg(\chi_{2,0})] - |\chi_{1,0}||\chi_{3,0}|S^0_{22}\sigma\sin[2(\beta+\omega\tau)+\arg(\chi_{1,0})+\arg(\chi_{3,0})])}{1+|\chi_{1,0}|^2|\chi_{2,0}|^2|\chi_{3,0}|^2\sigma^6 - 2|\chi_{1,0}||\chi_{2,0}||\chi_{3,0}|\sigma^3\cos[3(\beta+\omega\tau)+\arg(\chi_{1,0})+\arg(\chi_{2,0})+\arg(\chi_{3,0})]},\\
\mathrm{Re}[S_{31}](\omega) &= \mathrm{Re}[S_{13}](\omega)\\
&= \frac{\sigma(|\chi_{3,0}|(S^0_{11}+|\chi_{1,0}|^2S^0_{22}\sigma^2)\cos[\beta+\omega\tau+\arg(\chi_{3,0})] + |\chi_{1,0}||\chi_{2,0}|S^0_{33}\sigma\cos[2(\beta+\omega\tau)+\arg(\chi_{1,0})+\arg(\chi_{2,0})])}{1+|\chi_{1,0}|^2|\chi_{2,0}|^2|\chi_{3,0}|^2\sigma^6 - 2|\chi_{1,0}||\chi_{2,0}||\chi_{3,0}|\sigma^3\cos[3(\beta+\omega\tau)+\arg(\chi_{1,0})+\arg(\chi_{2,0})+\arg(\chi_{3,0})]},\\
\mathrm{Im}[S_{31}](\omega) &= -\mathrm{Im}[S_{13}](\omega)\\
&= \frac{\sigma(|\chi_{3,0}|(S^0_{11}+|\chi_{1,0}|^2S^0_{22}\sigma^2)\sin[\beta+\omega\tau+\arg(\chi_{3,0})] - |\chi_{1,0}||\chi_{2,0}|S^0_{33}\sigma\sin[2(\beta+\omega\tau)+\arg(\chi_{1,0})+\arg(\chi_{2,0})])}{1+|\chi_{1,0}|^2|\chi_{2,0}|^2|\chi_{3,0}|^2\sigma^6 - 2|\chi_{1,0}||\chi_{2,0}||\chi_{3,0}|\sigma^3\cos[3(\beta+\omega\tau)+\arg(\chi_{1,0})+\arg(\chi_{2,0})+\arg(\chi_{3,0})]}.
\end{aligned}
\tag{B.1}
$$

(regularity). This coherence resonance can be enhanced by tuning the coupling strength appropriately.

Eventually, we have demonstrated that the characteristic profile of multiple resonance peaks within the spectra persists in the case of delay-coupled heterogeneous Hopf normal forms if the frequency detuning between the oscillators is not too large. Due to the heterogeneities, the spectra become asymmetric and frequency shifted, but the delay-induced deterministic oscillation patterns, which cause the multiple resonance peaks, can still be observed. Consequently, the main characteristics of these spectra are robust against moderate local heterogeneities.

Interesting extensions of our work concern the application of the general theory to larger networks of nonlinear oscillators or the inclusion of common and/or colored instead of white noise (then the individual nodes would not be independent anymore, and there might also be temporal correlations in the noise). Further, an interesting application of our theory would be the analytical calculation of emission spectra in models of so-called oto-acoustic emissions, which are self-generated tones in the inner-ear organs of vertebrates. This fascinating phenomenon has been described by arrays of noisy nonlinear oscillators (see, e.g. [41]) and is thus accessible to the kind of analysis we have presented in this paper.

This work was supported by DFG in the framework of SFB 910 and by the BMBF (FKZ: 01GQ1001A).

Appendix A

The power spectral density PSD S_{kk} and cross-spectral densities CS S_{kj} of two symmetrically coupled nonlinear oscillators (Eqs. (1) and (14)) is given by:

see equation (A.1) *above*

where $k \neq j$, $k, j = 1, 2$, $\arg(\cdot)$ denotes the argument (phase) and $|\cdot|$ the modulus of a complex number.

Appendix B

The PSD S_{kk} and CS S_{kj} ($k \neq j$ and $k, j = 1, 2, 3$) of three asymmetrically coupled nonlinear oscillators (Eqs. (1) and (20)) is given by:

see equation (B.1) *above.*

References

1. M.C. Soriano, J. García-Ojalvo, C.R. Mirasso, I. Fischer, Rev. Mod. Phys. **85**, 421 (2013)
2. N. Brunel, V. Hakim, Chaos **18**, 015113 (2008)
3. S. Ares, L.G. Morelli, D.J. Jörg, A.C. Oates, F. Jülicher, Phys. Rev. Lett. **108**, 204101 (2012)
4. S. Yanchuk, P. Perlikowski, Phys. Rev. E **79**, 046221 (2009)
5. O. D'Huys, R. Vicente, T. Erneux, J. Danckaert, I. Fischer, Chaos **18**, 037116 (2008)
6. C.U. Choe, T. Dahms, P. Hövel, E. Schöll, Phys. Rev. E **81**, 025205(R) (2010)
7. R. Vicente, L.L. Gollo, C.R. Mirasso, I. Fischer, P. Gordon, Proc. Natl. Acad. Sci. USA **105**, 17157 (2008)
8. G. Hu, T. Ditzinger, C.Z. Ning, H. Haken, Phys. Rev. Lett. **71**, 807 (1993)
9. A.S. Pikovsky, J. Kurths, Phys. Rev. Lett. **78**, 775 (1997)
10. A. Neiman, P.I. Saparin, L. Stone, Phys. Rev. E **56**, 270 (1997)
11. B. Lindner, J. García-Ojalvo, A. Neiman, L. Schimansky-Geier, Phys. Rep. **392**, 321 (2004)
12. O.V. Ushakov, H.J. Wünsche, F. Henneberger, I.A. Khovanov, L. Schimansky-Geier, M.A. Zaks, Phys. Rev. Lett. **95**, 123903 (2005)
13. A. Zakharova, T. Vadivasova, V. Anishchenko, A. Koseska, J. Kurths, Phys. Rev. E **81**, 011106 (2010)
14. A. Zakharova, A. Feoktistov, T. Vadivasova, E. Schöll, Eur. Phys. J. Special Topics **222**, 2481 (2013)
15. N.B. Janson, A.G. Balanov, E. Schöll, Phys. Rev. Lett. **93**, 010601 (2004)
16. G. Stegemann, A.G. Balanov, E. Schöll, Phys. Rev. E **73**, 016203 (2006)
17. B. Hauschildt, N.B. Janson, A.G. Balanov, E. Schöll, Phys. Rev. E **74**, 051906 (2006)
18. S.A. Brandstetter, M.A. Dahlem, E. Schöll, Phil. Trans. R. Soc. A **368**, 391 (2010)
19. F. Jülicher, K. Dierkes, B. Lindner, J. Prost, P. Martin, Eur. Phys. J. E **29**, 449 (2009)
20. B. Doiron, B. Lindner, A. Longtin, L. Maler, J. Bastian, Phys. Rev. Lett. **93**, 048101 (2004)
21. B. Lindner, B. Doiron, A. Longtin, Phys. Rev. E **72**, 061919 (2005)
22. J. Trousdale, Y. Hu, E. Shea-Brown, K. Josić, PLoS Comp. Biol. **8**, 1 (2012)
23. N. Sharafi, J. Benda, B. Lindner, J. Comp. Neurosci. **34**, 285 (2013)
24. V. Flunkert, E. Schöll, Phys. Rev. E **76**, 066202 (2007)
25. S. Wieczorek, B. Krauskopf, T. Simpson, D. Lenstra, Phys. Rep. **416**, 1 (2005)
26. R.J. Olsen, I.R. Epstein, J. Chem. Phys. **98**, 2805 (1993)
27. J. Kosek, P.G. Sorensen, M. Marek, F. Hynne, J. Phys. Chem. **98**, 6128 (1994)
28. R. FitzHugh, Biophys. J. **1**, 445 (1961)
29. T. Kostova, R. Ravindran, M. Schonbek, Int. J. Bifurc. Chaos **14**, 913 (2004)
30. K. Tsumoto, K. Kitayama, T. Yoshinaga, K. Aihara, H. Kawakami, Neurocomputing **69**, 293 (2006)
31. Y. Choe, M.O. Magnasco, A.J. Hudspeth, Proc. Natl. Acad. Sci. USA **95**, 1532 (1998)
32. A.J. Hudspeth, Neuron **59**, 530 (2008)
33. D.A. Arroyo-Almanza, A.N. Pisarchik, I. Fischer, C.R. Mirasso, M.C. Soriano, Opt. Commun. **301-302**, 67 (2013)
34. S.A. Campbell, *Handbook of Brain Connectivity* (Springer-Verlag, Berlin, 2007)
35. N. Bleistein, R.A. Handelsman, *Asymptotic Expansions of Integrals* (Dover Publications, New York, 2010)
36. B. Lindner, K. Dierkes, F. Jülicher, Phys. Rev. Lett. **103**, 250601 (2009)
37. A.G. Balanov, N.B. Janson, E. Schöll, Physica D **199**, 1 (2004)
38. J. Pomplun, A. Amann, E. Schöll, Europhys. Lett. **71**, 366 (2005)
39. Y.-Y. Liu, G.-Q. Xia, T. Deng, Y. He, Z.-M. Wu, J. Optoel. Adv. Mater. **13**, 613 (2011)
40. Y. Aviad, I. Reidler, M. Zigzag, M. Rosenbluh, I. Kanter, Opt. Express **20**, 4352 (2012)
41. A. Vilfan, T. Duke, Biophys. J. **95**, 4622 (2008)